Inorganic Chemistry

Article

pubs.acs.org/IC

One-Dimensional and Two-Dimensional Anilate-Based Magnets with Inserted Spin-Crossover Complexes

Alexandre Abhervé, Miguel Clemente-León,* Eugenio Coronado,* Carlos J. Gómez-García, and Martin Verneret

Instituto de Ciencia Molecular (ICMol), Universidad de Valencia, Catedrático José Beltrán 2, 46980 Paterna, Spain

Supporting Information

ABSTRACT: The syntheses, structures, and magnetic properties of a family of bimetallic anilate-based compounds with inserted spin-crossover cationic complexes are reported. The structures of **1**−**4** present a two-dimensional anionic network formed by Mn(II) and Cr(III) ions linked through anilate ligands with inserted $[Fe^{III}(sal_2\text{-trien})]^+$ (**1**), $[Fe^{III}(4\text{-OH-sal}_2\text{-trien})]^+$ (**2**), $[Fe^{III}(sal_2\text{-epe})]^+$ (**3**), or $[Fe^{III}(5\text{-Cl-sal}_2\text{-trien})]^+$ (**4**) complexes. The structure of **5** is formed by anionic $[Mn^{II}Cl_2Cr^{III}(Cl_2An)_3]^{3-}$ chains surrounded by $[Fe^{II}(tren(imid)_3)]^{2+}$, Cl^-, and solvent molecules. The magnetic properties indicate that **1**−**4** undergo a long-range ferrimagnetic ordering at ca. 10 K. On the other hand, the inserted Fe(III) cations remain in the low-spin (in **4**) or high-spin state (in **1**, **2**, and **3**). In the case of **5**, half of the inserted Fe(II) cations undergo a complete and gradual spin crossover from 280 to 90 K that coexists with a magnetic ordering below 2.5 K.

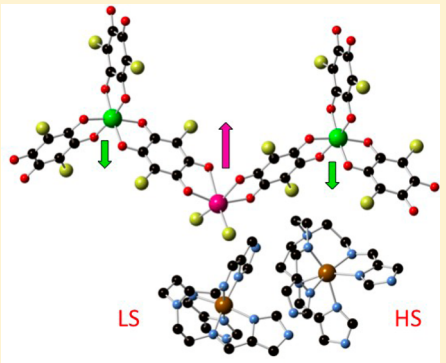

INTRODUCTION

Multifunctionality is one of the most appealing topics in chemical science. A rational approach to design hybrid multifunctional materials consists of the controlled assembly of two functional networks incorporating two properties or contributing synergistically to the appearance of new physical phenomena.[1] Among the later class of materials, those responding to an external stimulus are attracting considerable interest in view of their potential applications as chemical switches, memory or molecular sensors.[2] In this context, two-network compounds formed by a magnetic lattice and a switchable molecular component are promising candidates for the preparation of responsive magnetic materials.

Spin-crossover complexes are particularly suitable as switchable molecular components because they represent one of the best examples of molecular bistability. These molecular complexes change their spin state from low-spin (LS) to high-spin (HS) configurations under an external stimulus such as temperature, light irradiation, or pressure.[3] As this is accompanied by changes in the molecular size, the spin-crossover process should act as an internal pressure in the hybrid material, and therefore, it might affect the long-range magnetic ordering in the extended magnetic network.

Bimetallic oxalate-bridged compounds have been thoroughly used as magnetic lattice of multifunctional magnetic materials. They are formed by polymeric anionic networks $[M^{II}M^{III}(ox)_3]^-$ (ox = oxalate) with magnetic ions linked through bis-bidentate bridging oxalate ligands. The use of different charge-compensating molecular cations, which template the network formation, has provided many examples of multifunctional materials,[4] combining the long-range magnetic ordering of the oxalate network with paramagnetism,[5] photochromism,[6] electrical conductivity,[7] proton conductivity,[8] ferroelectricity,[9] chirality,[10] or single-molecule magnet behavior from the cation.[11] Fe(II) and Fe(III) spin-crossover cationic complexes have been used for the growth of two-dimensional (2D) and three-dimensional (3D) bimetallic oxalate-based magnets in the search of responsive magnetic materials.[12] Fe(II) spin-crossover complexes have led to the growth of 3D bimetallic oxalate-based compounds, which present magnetic properties very sensitive to the changes in size of the inserted cation, although the inserted Fe(II) complexes do not present a clear spin-crossover behavior.[12g,13] The most interesting results were obtained for the family of compounds $[Fe^{III}(sal_2\text{-trien})][Mn^{II}Cr^{III}(ox)_3]\cdot G$ (G = CH_2Cl_2, $CHBr_3$, CH_2Br_2, and $CHCl_3$, H_2 Sal_2-trien = *N*,*N*′-disalicylidenetriethylene-tetramine, see Scheme 1) formed by alternating layers of a 2D oxalate-based network, $[Fe^{III}(sal_2\text{-trien})]^+$ complexes and solvent molecules.[12b,e,h] They show that the confinement of spin-crossover cations into extended networks induce an unexpected property, a photoinduced spin-crossover transition of the inserted complex (LIESST effect), something very unusual for Fe(III) complexes. Unfortunately, the photo-induced spin conversion of the inserted Fe(III) complex has a negligible influence on the magnetic behavior of the 2D oxalate network as the magnetic ordering of this type of network is not sensitive to the change in size of the inserted cation.

Motivated by the interesting results obtained with bimetallic oxalate-based networks, we have attempted the use of larger bis-bidentate bridging ligands as the 2,5-dihydroxy-1,4-benzoquinone dianion derivatives of formula $C_6O_4X_2^{2-}$

Received: July 14, 2014
Published: October 28, 2014

dx.doi.org/10.1021/ic5016803 | *Inorg. Chem.* 2014, 53, 12014−12026

Scheme 1. Ligands of the Fe(III) and Fe(II) Complexes

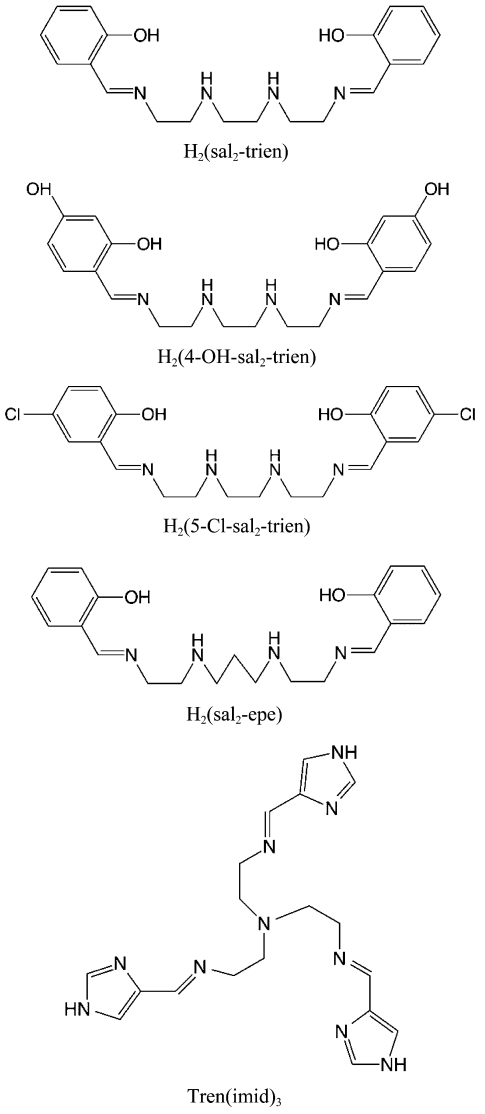

(X_2An^{2-}; X = Cl or Br, see Scheme 2). These ligands, which show coordination modes similar to the oxalate ligand, present additional advantages: (i) they are easy to modify or functionalize by simply changing the X group; (ii) they present higher ordering temperatures, T_c's; (iii) their bigger size may enable the introduction of a larger library of cations in order to prepare multifunctional molecular materials. The first example of this kind, obtained by our group, is the family of layered ferrimagnets $A[M^{II}M^{III}(X_2An)_3]\cdot G$ (A = $[(H_3O)(phz)_3]^+$ (phz = phenazine) or NBu_4^+; X = H, Cl, Br, I; G = water or acetone) with T_c ranging from 5.5 to 11.0 K and which, depending on the X substituent, can be porous and/or chiral.[14a]

Scheme 2. 2,5-Dihydroxy-1,4-benzoquinone Dianion Derivatives Used in This Work

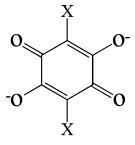

X_2An^{2-}; X = Cl or Br

In this work, we explore the use of the Fe(III) complexes, $[Fe^{III}(sal_2\text{-trien})]^+$, $[Fe^{III}(4\text{-OH-sal}_2\text{-trien})]^+$, $[Fe^{III}(sal_2\text{-epe})]^+$, and $[Fe^{III}(5\text{-Cl-sal}_2\text{-trien})]^+$ derivatives, and the Fe(II) complex, $[Fe^{II}(tren(imid)_3)]^{2+}$ (see Scheme 1) for the preparation of multifunctional compounds based on the anilate-based network in the search of new compounds combining spin-crossover and magnetic ordering. The first results of this strategy are reported in this paper.

EXPERIMENTAL SECTION

General Remarks. The Fe(III) complexes[15,16] and $[Fe^{II}(tren(imid)_3)](BF_4)_2$ were prepared according to literature methods.[17] $[(n\text{-}Bu)_4N]_3[Cr^{III}(X_2An)_3]$ (X=Cl, Br) was prepared by a modification of the literature method.[14] All other materials and solvents were commercially available and used without further purification.

Synthesis of $[NBu_4]_3[Cr^{III}(Cl_2An)_3]$ and $[NBu_4]_3[Cr^{III}(Br_2An)_3]$. An aqueous solution (10 mL) of $CrCl_3\cdot 6H_2O$ (400 mg, 1.5 mmol) was added dropwise to an aqueous solution (30 mL) of H_2Cl_2An or H_2Br_2An (5 mmol), NaOH (400 mg, 10 mmol), and NBu_4Br (1.6 g, 5 mmol). After 30 min at 70 °C, the mixture was allowed to cool to room temperature and extracted three times with 75 mL of CH_2Cl_2. The CH_2Cl_2 solution was dried with Na_2SO_4, filtered, rotoevaporated to dryness, and crystallized in dimethylformamide to give red shiny crystals after 2 weeks.

Synthesis of $[Fe^{III}(sal_2\text{-trien})][Mn^{II}Cr^{III}(Cl_2An)_3]\cdot(CH_2Cl_2)_{0.5}\cdot(CH_3OH)\cdot(H_2O)_{0.5}\cdot(CH_3CN)_5$ (1), $[Fe^{III}(4\text{-OH-sal}_2\text{-trien})][Mn^{II}Cr^{III}(Cl_2An)_3]\cdot$(solvate) (2), $[Fe^{III}(sal_2\text{-epe})][Mn^{II}Cr^{III}(Br_2An)_3]\cdot(CH_3CN)_4\cdot$(solvate) (3), $[Fe^{III}(5\text{-Cl-sal}_2\text{-trien})][Mn^{II}Cr^{III}(Br_2An)_3]\cdot(CH_2Cl_2)\cdot(CH_3OH)\cdot(H_2O)_4\cdot(CH_3CN)_{1.5}\cdot$(solvate) (4), and $[Fe^{II}(tren(imid)_3)]_2[Mn^{II}Cl_2Cr^{III}(Cl_2An)_3]Cl\cdot(CH_3OH)\cdot(CH_2Cl_2)_3\cdot(CH_3CN)_{0.5}$ (5). Crystals of these compounds were obtained by slow diffusion of two solutions. The first solution was prepared by dissolving $MnCl_2\cdot 4H_2O$ (12 mg, 0.06 mmol) and the Fe(III) complexes (0.06 mmol) in 6 mL of a 9:1 dichloromethane/methanol mixture ($[Fe^{III}(sal_2\text{-trien})](PF_6)$ (32 mg) for **1**, $[Fe^{III}(4\text{-OH-sal}_2\text{-trien})]Cl$ (27 mg) for **2**, $[Fe^{III}(sal_2\text{-epe})](ClO_4)$ (31 mg) for **3**, and $[Fe^{III}(5\text{-Cl-sal}_2\text{-trien})](PF_6)$ (38 mg) for **4**). In the case of **5**, it is necessary to dissolve first the $[Fe^{II}(tren(imid)_3)](BF_4)_2$ complex (73 mg, 0.12 mmol) in 6 mL of a 2:1 dichloromethane/methanol mixture and then add $MnCl_2\cdot 4H_2O$ (12 mg, 0.06 mmol). The second solution was obtained by dissolving $[NBu_4]_3[Cr^{III}(Cl_2An)_3]$ (84 mg, 0.06 mmol, for **1**, **2**, and **5**) or $[NBu_4]_3[Cr^{III}(Br_2An)_3]$ (100 mg, 0.06 mmol, for **3** and **4**) in 6 mL of acetonitrile. After 2–4 weeks, black prismatic single crystals suitable for X-ray crystal analysis were obtained. Yields: 6.8% (**1**), 6.8% (**2**), 7.4% (**3**), 5.4% (**4**), and 11.1% (**5**). These yields could be improved by diffusing the two solutions for longer times. Anal. Calcd for $C_{38.5}H_{37}Cl_7CrFeMnN_4O_{20}$ (**1**) (with 0.5 dichloromethane molecule and 6 water molecules per formula in the structure due to desolvation and rehydratation): C, 35.6; H, 3.1; N, 4.4%. Found: C, 35.9; H, 2.9; N, 4.4%. Anal. Calcd for $C_{38}H_{56}Cl_6CrFeMnN_4O_{32}$ (**2**) (with 16 water molecules per formula in the structure due to partial desolvation): C, 31.3; H, 3.9; N, 3.8%. Found: C, 31.4; H, 3.5; N, 4.3%. Anal. Calcd for $C_{39}H_{26}Br_6CrFeMnN_4O_{14}$ (**3**) (with no solvent molecules in the structure due to complete desolvation): C, 33.1; H, 1.8; N, 4.0%. Found: C, 32.4; H, 2.0; N, 4.0%. Anal. Calcd for $C_{43}H_{40.5}Br_6Cl_4CrFeMnN_{5.5}O_{19}$ (**4**): C, 30.0; H, 2.4; N, 4.5%. Found: C, 30.7; H, 2.1; N, 3.7%. Anal. Calcd for $C_{58}H_{55.5}Cl_{13}CrFe_2MnN_{20.5}O_{13}$ (**5**): C, 36.1; H, 2.9; N, 14.9%. Found: C, 35.5; H, 1.7; N, 14.1%. IR (KBr pellet) for **1**: 1624 (s), 1590 (sh), 1506 (vs), 1398 (w), 1359 (vs), 1305 (sh), 1007 (m), 835 (m) cm^{-1}. IR (KBr pellet) for **2**: 1625 (s), 1542 (sh), 1516 (vs), 1400 (m), 1360 (vs), 1007 (m), 849 (m) cm^{-1}. IR (KBr pellet) for **3**: 1623 (s), 1540 (sh), 1509 (sh), 1491 (vs), 1400 (m), 1351 (vs), 989 (m), 817 (m) cm^{-1}. IR (KBr pellet) for **4**: 1629 (s), 1517 (sh), 1491 (vs), 1401 (m), 1352 (vs), 990 (m), 817 (m) cm^{-1}. IR (KBr pellet) for **5**: 1635 (vs), 1533 (vs), 1507 (sh), 1401 (m), 1356 (vs), 1005 (m), 848 (m) cm^{-1}.

dx.doi.org/10.1021/ic5016803 | Inorg. Chem. 2014, 53, 12014–12026

Table 1. Crystallographic Data for Compounds 1, 2 and 3

compd	1	2	3
empirical formula	$C_{49.5}H_{40}Cl_7CrFeMnN_9O_{15.5}$	$C_{38}H_{24}Cl_6CrFeMnN_4O_{16}$	$C_{47}H_{26}Br_6CrFeMnN_8O_{14}$
fw	1419.84	1168.10	1569.01
cryst color	black	black	black
cryst size	0.2 × 0.08 × 0.04	0.10 × 0.08 × 0.06	0.16 × 0.08 × 0.06
temp (K)	120(2)	120(2)	120(2)
wavelength (Å)	0.71073	0.71073	0.71073
cryst syst, Z	monoclinic, 4	hexagonal, 3	monoclinic, 4
space group	$C\ 222_1$	$P\ 6_122$	$P\ 2_1/c$
a (Å)	12.9780(6)	13.7059(2)	14.1383(7)
b (Å)	24.8692(12)	13.7059(2)	22.3075(10)
c (Å)	21.9676(9)	66.2433(10)	23.4765(11)
α (deg)	90	90	90
ß (deg)	90	90	103.200(5)
γ (deg)	90	120	90
V (Å^3)	7090.1(6)	10776.7(4)	7208.6(6)
ρ_{calc}(Mg/m^3)	1.330	1.081	1.446
μ(Mo Kα) (mm^{-1})	0.852	0.791	3.899
θ range (deg)	2.916−27.597	3.205−25.081	2.892−26.048
reflns collected	81831	180425	117721
independent reflns (R_{int})	8183 (0.1702)	7375 (0.2011)	7113 (0.2088)
L. S. parameters, p/restraints, r	355/1	223/0	659/24
absolute structure parameter	0.076(19)	0.19(10)	
$R1(F)$,[a] $I > 2\sigma(I)$	0.0935	0.1354	0.1505
$wR2(F^2)$,[b] all data	0.2815	0.3273	0.4105
$S(F^2)$,[c] all data	1.029	0.827	1.011

[a] $R1(F) = \Sigma||F_0|-|F_C||/\Sigma|F_0|$; [b] $wR2(F^2) = [\Sigma w(F_0^2-F_C^2)^2/\Sigma wF_0^4]^{1/2}$; [c] $S(F^2) = [\Sigma w(F_0^2-F_C^2)^2/(n + r - p)]^{1/2}$.

Table 2. Crystallographic Data for Compounds 4, 5 at 120 K and 5 at 220 K

compd	4	5 (120 K)	5 (220 K)
empirical formula	$C_{43}H_{40.5}Br_6Cl_4CrFeMnN_{5.5}O_{19}$	$C_{59}H_{59.5}Cl_{15}CrFe_2MnN_{20.5}O_{13}$	$C_{58}H_{57.5}Cl_{13}CrFe_2MnN_{20.5}O_{13}$
fw	1722.32	2014.16	1927.22
cryst color	black	black	black
cryst size	0.16 × 0.09 × 0.06	0.11 × 0.09 × 0.07	0.12 × 0.09 × 0.06
temp (K)	120(2)	120(2)	120(2)
wavelength (Å)	0.71073	0.71073	0.71073
cryst syst, Z	monoclinic, 4	triclinic, 2	triclinic, 2
space group	$P\ 2_1/c$	P-1	P-1
a (Å)	13.9066(8)	13.2167(3)	13.2687(6)
b (Å)	23.1892(9)	16.2053(4)	16.5753(4)
c (Å)	22.7189(13)	20.2599(5)	20.3252(7)
α (deg)	90	97.796(2)	98.056(3)
ß (deg)	101.422(6)	97.354(2)	98.056(3)
γ (deg)	90	95.928(2)	95.922(3)
V (Å^3)	7181.4(7)	4231.55(18)	4347.9(3)
ρ_{calc} (Mg/m^3)	1.552	1.581	1.472
μ(Mo Kα) (mm^{-1})	4.066	1.148	1.054
θ range (deg)	2.985−26.427	2.955−27.502	2.849−26.483
reflns collected	113316	62029	69165
independent reflns (R_{int})	7832 (0.2296)	19299 (0.0887)	7112 (0.1373)
L. S. parameters, p/restraints, r	706/0	1048/0	817/8
$R1(F)$,[a] $I > 2\sigma(I)$	0.1618	0.0812	0.1101
$wR2(F^2)$,[b] all data	0.4331	0.2649	0.3631
$S(F^2)$,[c] all data	1.064	1.037	1.031

[a] $R1(F) = \Sigma||F_0|-|F_C||/\Sigma|F_0|$; [b] $wR2(F^2) = [\Sigma w(F_0^2-F_C^2)^2/\Sigma wF_0^4]^{1/2}$; [c] $S(F^2) = [\Sigma w(F_0^2-F_C^2)^2/(n + r - p)]^{1/2}$.

Structural Characterization. Single crystals of all compounds were mounted on glass fibers using a viscous hydrocarbon oil to coat the crystal and then transferred directly to the cold nitrogen stream for data collection. All reflection data were collected at 120 K for **1**−**4** and at 120 and 220 K for **5** on a Supernova diffractometer equipped with a graphite-monochromated Enhance (Mo) X-ray Source (λ = 0.7107 Å). The CrysAlisPro program, Oxford Diffraction Ltd., was used for unit cell determinations and data reduction. Empirical absorption correction was performed using spherical harmonics, implemented in the SCALE3 ABSPACK scaling algorithm. Crystal structures were

dx.doi.org/10.1021/ic5016803 | Inorg. Chem. 2014, 53, 12014−12026

solved by direct methods with the SIR97 program[18] and refined against all F^2 values with the SHELXL-2013 program[19] using the WinGX graphical user interface.[20] All non-hydrogen atoms were refined anisotropically except as noted, and hydrogen atoms were placed in calculated positions and refined isotropically with a riding model. Data collection and refinement statistics are collected in Tables 1 and 2. The structure of **5** at 220 K showed a weak diffraction due to the loss of CH_2Cl_2 solvent molecules from the structure. As a result of this weak diffraction, it was not possible to refine anisotropically C atoms from $[Fe^{II}(tren(imid)_3)]^{2+}$ complexes. Furthermore, this caused a smaller number of CH_2Cl_2 molecules in the structure solved at 220 K compared with that solved at 120 K (see Table 2). The subroutine SQUEEZE from PLATON[21] was used to calculate and remove the diffracting component of disordered solvents in **2**, **3**, and **4**, resulting in a void of ca. 5383 Å^3 and 1537 electrons/cell for **2**, in two voids of ca. 314 Å^3 and ca. 90 electrons/cell plus six smaller voids of less than 41 Å^3 and 7 electrons/cell for **3**, and two voids of ca. 307 Å^3 and 96 electrons/cell plus four smaller voids of less than 54 Å^3 and 20 electrons/cell for **4**. This corresponds to ca. 23 H_2O molecules per asymmetric unit for **2**, ca. 2 CH_3CN molecules per asymmetric unit for **3**, and 1 CH_3OH + 2 CH_3CN molecule per asymmetric unit for **4**. The CH_3OH molecule from the smallest voids of **4** has been included in the formula of the compound in Table 2 and Supporting Information (see cif file). CCDC-998895 to 998898, 1003585, and 1004948 contain the supplementary crystallographic data for this paper. These data can be obtained free of charge from The Cambridge Crystallographic Data Centre via www.ccdc.cam.ac.uk/data_request/cif. Glass capillaries (0.5 mm) were filled with polycrystalline samples of the compounds and mounted and aligned on a Empyrean PANalytical powder diffractometer, using Cu Kα radiation (λ = 1.54177 Å). A total of two scans were collected at room temperature in the 2θ range 5−40°.

Physical Measurements. Magnetic measurements were performed with a Quantum Design MPMS-XL-5 SQUID magnetometer in the 2 to 300 K temperature range with an applied magnetic field of 0.1 T on polycrystalline samples. The AC measurements were performed in the temperature range of 2−15 K at different frequencies with an oscillating magnetic field of 0.395 mT. The magnetization and hysteresis studies were performed between 5 and −5 K T, cooling the samples at zero field. Infrared (IR) spectra were recorded on a FTIR 320 Nicolet spectrometer. C, H, and N elemental analyses were measured on a CE Instruments EA 1110 CHNS Elemental analyzer. The Fe/Mn/Cr/Cl and Fe/Mn/Cr/Br/Cl ratios were measured with a Philips ESEM X230 scanning electron microscope equipped with an EDAX DX-4 microsonde.

RESULTS AND DISCUSSION

Synthesis. The compounds of formula $[Fe^{III}(sal_2\text{-trien})][Mn^{II}Cr^{III}(Cl_2An)_3]\cdot(CH_2Cl_2)_{0.5}\cdot(CH_3OH)\cdot(H_2O)_{0.5}\cdot(CH_3CN)_5$ (**1**), $[Fe^{III}(4\text{-OH-sal}_2\text{-trien})][Mn^{II}Cr^{III}(Cl_2An)_3]\cdot$(solvate) (**2**), $[Fe^{III}(sal_2\text{-epe})][Mn^{II}Cr^{III}(Br_2An)_3]\cdot(CH_3CN)_4\cdot$(solvate) (**3**), $[Fe^{III}(5\text{-Cl-sal}_2\text{-trien})][Mn^{II}Cr^{III}(Br_2An)_3]\cdot(CH_2Cl_2)\cdot(CH_3OH)\cdot(H_2O)_4\cdot(CH_3CN)_{1.5}\cdot$(solvate) (**4**), and $[Fe^{II}(tren(imid)_3)]_2\ [Mn^{II}Cl_2Cr^{III}(Cl_2An)_3]Cl\cdot(CH_3OH)\cdot(CH_2Cl_2)_3\cdot(CH_3CN)_{0.5}$ (**5**) have been prepared and characterized. The method to prepare these anilate-based compounds differs from that used to prepare oxalate-based compounds with similar templating cations.[12] Oxalate-based compounds were obtained in most cases by the slow diffusion of a solution of the Fe(III) or Fe(II) complex into a solution containing the precursors of the oxalate network almost free of other counterions. This was possible thanks to the use of the Ag^+ salt of the $[Cr^{III}(ox)_3]^{3-}$ complex and $MnCl_2$ which enables the removal of Ag^+ and Cl^- counterions by precipitation of AgCl. In the case of the anilate-based compounds, a similar strategy could not be used due to poor stability of the Ag^+ salts of $[Cr^{III}(X_2An)_3]^{3-}$ complexes. $[NBu_4]^+$ salts of $[Cr^{III}(Cl_2An)_3]^{3-}$ and $[Cr^{III}(Br_2An)_3]^{3-}$ were chosen instead because they can be obtained with a high degree of purity, something very important for the crystallization of the compounds. On the other hand, because the mixture of $[NBu_4]_3[Cr^{III}(Cl_2An)_3]$ or $[NBu_4]_3[Cr^{III}(Br_2An)_3]$ and $MnCl_2$ in the same solvent gives rise to a fast precipitation of the 2D compound, $[NBu_4][Mn^{II}Cr^{III}(X_2An)_3]$ (X = Cl or Br), the two precursors of the anilate-based network were dissolved in different solvents. The best results were obtained mixing $MnCl_2$ with the Fe(III) or Fe(II) complex in methanol/dichloromethane and slowly diffusing this solution into an acetonitrile solution of $[(n\text{-}Bu)_4N]_3[Cr^{III}(Cl_2An)_3]$ or $[(n\text{-}Bu)_4N]_3[Cr^{III}(Br_2An)_3]$. Other solvent mixtures with the same templating cations (chloroform in the place of dichloromethane or methanol in the place of acetonitrile) gave rise to other phases with a similar structure that will be reported in future works. In the case of **5**, it was necessary to dissolve the Fe(II) complex first in the methanol/dichloromethane mixture and then add the $MnCl_2\cdot4H_2O$ salt. The excess of Mn^{2+} resulting from an addition of the Fe(II) complex to a methanol solution of $MnCl_2\cdot4H_2O$ gives rise to the partial substitution of Fe(II) by Mn(II) in the tren(imid)$_3$ complex of the final compound. This was not observed in the other compounds of this paper. Furthermore, in contrast to **1**, **2**, **3**, and **4**, the Cl^- anions from $MnCl_2$ in **5** are coordinated to Mn(II) and act as counterions. The use of other Mn(II) salts to avoid the presence of Cl^- in the structure did not result in suitable crystals for X-ray diffraction. The composition of crystals of these compounds was checked by elemental analysis and microanalysis. C, H, and N elemental analyses show differences with respect to the calculated values using the formulas obtained from X-ray diffraction data at 120 K, in the case of **1**, **2**, and **3**. These differences may be explained by the loss of solvent molecules when the crystals are extracted from the mother liquor at room temperature. Indeed, a good coincidence between experimental and calculated values is obtained by decreasing the number of solvent molecules in these three structures (see above). Moreover in the case of **1**, the low nitrogen and carbon contents could indicate rehydration with water. Thermal gravimetry analysis should be performed to clarify this point, but it was not possible due to the small amount of sample available. Microanalysis shows a Fe/Mn/Cr/Cl ratio close to 1:1:1:7 for **1**, 1:1:1:6 for **2**, and 2:1:1:9 for **5**, a Fe/Mn/Cr/Br ratio close to 1:1:1:6 for **3**, and a Fe/Mn/Cr/Cl/Br ratio close to 1:1:1:3:6 for **4**. The results obtained for compound **5** indicate that CH_2Cl_2 solvent molecules observed in the crystal structure are lost after extracting the crystals from the mother liquor.

Structures. The structures of all compounds have been solved by single-crystal X-ray diffraction. The structures of **1**, **2**, **3**, and **4** consist of bimetallic anionic layers with a 2D bimetallic X_2An (X=Cl or Br) network of formula $[Mn^{II}Cr^{III}(X_2An)_3]$ with inserted Fe(III) cationic complexes and solvent molecules. The bimetallic anilate layer presents in these four compounds the well-known honeycomb structure, which is similar to that found for other extended oxalate or anilate-based networks.[14a] It consists in a hexagonal layer where the Cr(III) and Mn(II) ions occupy alternating vertices of the hexagons and are linked through X_2An bridges in such a way that each Mn(II) is surrounded by three neighboring Cr(III) and vice versa. This contrasts with the oxalate-based compounds obtained with similar Fe(III) cationic complexes that may present either 2D or 3D structures, depending on the substituent of the sal$_2$-trien ligand.[12] In this work, three types of 2D structures have been

dx.doi.org/10.1021/ic5016803 | Inorg. Chem. 2014, 53, 12014−12026

obtained that present a similar 2D anilate-based network. Still, important differences in the packing of the Fe(III) complexes and solvent molecules placed between these layers have been observed. They crystallize in orthorhombic (**1**), monoclinic (**3** and **4**), and hexagonal (**2**) space groups. A consequence of the replacement of oxalate by the larger bis-bidentate bridging X_2An^{2-} ligands is the presence of pores in the structures, which are filled with solvent molecules. Often these molecules are disordered. This has given rise to weak diffraction and quick loss of crystallinity due to fast evaporation of solvent molecules especially in compounds **2**, **3**, and **4**. As a result of this, powder X-ray diffraction patterns of **1**, **2**, **3**, and **4** do not show clear peaks. In contrast to the 2D compounds obtained with $[Fe^{III}(sal_2\text{-trien})]^+$ and derivatives, the use of the Fe(II) complex, $[Fe^{II}(tren(imid)_3)]^{2+}$, results in the formation of an anionic chain in compound **5**. This chain is formed by $[Cr^{III}(Cl_2An)_3]^{3-}$ complexes bonded to two Mn(II) ions through two bis-bidentate chloranilate bridges, whereas the third choranilate is a terminal one. The octahedral coordination of Mn(II) ions is completed with two chloride ions in cis. This type of structure has been found for other oxalate-based[4] and homometallic anilate-based compounds,[22] but it is the first time that it is obtained for heterometallic anilate-based networks. Again, the bimetallic oxalate-based compound obtained with the same complex presents a different structure, a very irregular 3D oxalate network with coexistence of bis(bidentate) and terminal oxalate ligands and solvent methanol molecules linked to heptacoordinated Mn(II) ions.[12g] It seems that $[Fe^{II}(tren(imid)_3)]^{2+}$ favors the presence of terminal oxalate or anilate ligands due to the formation of hydrogen bonds beween the NH groups from imidazole ligands and the two oxygens of the terminal oxalate or anilate ligand (see below). The powder X-ray diffraction pattern of **5** presents some differences with respect to the theorethical one obtained from single crystal X-ray diffraction data at 120 or 220 K, which may be attributed to the loss of solvent molecules (CH_2Cl_2) after extracting the crystals from the mother liquor already shown by micronalysis (see above and Figure S1 in the Supporting Information, SI).

Structure of $[Fe^{III}(sal_2\text{-trien})][Mn^{II}Cr^{III}(Cl_2An)_3]\cdot(CH_2Cl_2)_{0.5}\cdot(CH_3OH)\cdot(H_2O)_{0.5}\cdot(CH_3CN)_5$ (1). This compound crystallizes in the orthorhombic chiral space group $C222_1$. The structure is formed by bimetallic anionic sheets in the *ab* plane of formula $[Mn^{II}Cr^{III}(Cl_2An)_3]^-$ alternating with layers of $[Fe^{III}(sal_2\text{-trien})]^+$ cations (Figure 1). Acetonitrile, water, methanol, or dichloromethane solvent molecules occupy the holes between cationic and anionic layers.

The anionic layer presents the honeycomb structure mentioned above (Figure 2). The Mn(II) and Cr(III) are localized and clearly distinguishable as they present different bond distances with anilate ligands. Thus, there is one crystallographically independent Mn, with an occupancy of 0.5 and Mn−O bond lengths in the range of 2.136(8)−2.168(8) Å, and one crystallographically independent Cr, with an occupancy of 0.5 and Cr−O bond lengths in the range of 1.975(8)−1.984(8) Å. These are typical Cr−O and Mn−O bond lengths. The neighboring metal centers of these layers present alternated chirality as usual for this type of 2D networks. In the crystal of **1** used to solve the structure, all the Cr(III) ions adopt a Δ-configuration, whereas all the Mn(II) adopt the Λ-one. Therefore, the configuration of each metal ion is preserved in the neighboring anilate layers.

Because we have started from a racemic mixture of $[Cr(Cl_2An)_3]^{3-}$, crystals of the two enantiomers are expected

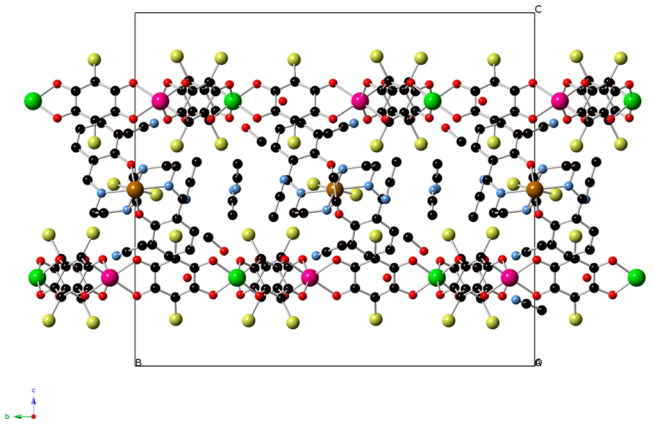

Figure 1. Projection of **1** in the *bc* plane. (Fe (brown), Cr (green), Mn (pink), C (black), N (blue), O (red), Cl (yellow). Hydrogen atoms have been omitted for clarity.

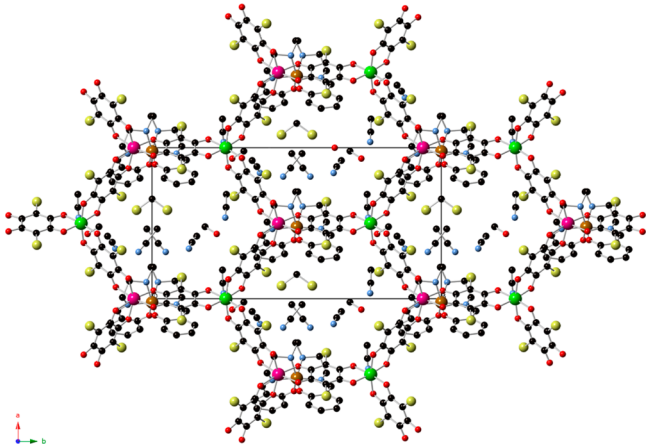

Figure 2. Projection of **1** in the *ab* plane showing one anionic layer and one cationic layer. (Fe (brown), Cr (green), Mn (pink), C (black), N (blue), O (red) Cl (yellow)). Hydrogen atoms have been omitted for clarity.

to be obtained. A similar behavior has been observed in other 2D oxalate and anilate structures.[8a,12c,f,14a] The chirality of the $[Fe^{III}(sal_2\text{-trien})]^+$ cations may be responsible of this first-order spontaneous resolution through chiral recognition between one of the enantiomers of $[Cr(Cl_2An)_3]^{3-}$ and $[Fe^{III}(sal_2\text{-trien})]^+$. In agreement with this, the crystallographically independent $[Fe^{III}(sal_2\text{-trien})]^+$ complex placed between the anilate layers adopts a Λ-configuration and interacts through several short contacts (see below) with the Cl_2An^{2-} ligands linked to Cr(III) from the upper and lower layers, which adopt the opposite configuration. As expected, given the larger size of the $[Fe^{III}(sal_2\text{-trien})]^+$ cation, the interlayer distance in **1** (10.98 Å), is significantly longer than those observed in the other anilate-based 2D compounds with $[(H_3O)(phz)_3]^+$ (in the range 9.03−9.21 Å) or NBu_4^+ cations (8.42 Å).[14a] This longer interlayer distance and the displacement of consecutive layers in the *ab* plane (due to the *C*-type unit cell) implies that the minimum distance between metals of different layers (11.423 Å) is also significantly longer than those found in the other anilate-based 2D compounds with NBu_4^+ (9.69 Å, where the layers are also displaced) or $[(H_3O)(phz)_3]^+$ cations (9.03−9.21 Å, where the layers are eclipsed).[14a] Albeit, this shortest metal−metal distance in **1** (11.423 Å) is similar to that

dx.doi.org/10.1021/ic5016803 | *Inorg. Chem.* 2014, 53, 12014−12026

observed in the compounds obtained by insertion of $[Fe^{III}(sal_2\text{-trien})]^+$ cations and derivatives into 2D bimetallic oxalate-based networks (11.609−12.807 Å).[12] A second consequence of the displacement of the consecutive layers is the formation of channels along the *c* axis (see Figure S2 in SI) that are occupied by solvent molecules.

The cationic layer intercalated between these anilate layers is formed by a crystallographically independent $[Fe^{III}(sal_2\text{-trien})]^+$ complex with an occupancy of 0.5 and solvent molecules. $[Fe^{III}(sal_2\text{-trien})]^+$ complexes are between two Mn atoms from the upper and lower anilate-based networks (see Figures 2 and S2 in the SI). The longer axis of the molecule is approximately perpendicular to the anilate-based layers with the atoms of the two phenolate rings of the complex parallel to one of the anilate ring of the two neighboring layers. Fe(III) complexes present a very distorted octahedral symmetry. SHAPE calculations show that the coordination geometry around Fe falls along the minimal distortion path between a perfect octahedron and a perfect trigonal prism with a deviation of less than 10%.[23] The generalized coordinate between the two ideal polyhedra is 50.1%. This indicates that the geometry of the $[Fe^{III}(sal_2\text{-trien})]^+$ complexes is intermediate between a trigonal prism and an octahedron. It seems that the insertion of these cations into anilate-based networks induces a larger distortion of the octahedral geometry compared with their insertion into 2D oxalate-based networks, as the maximum values of trigonal prismacity of 2D oxalate-base compounds with similar complexes are always lower than 41%.[12h] Average Fe−N and Fe−O bond lengths are 2.172(10) and 1.918(8) Å, which are in the range of those obtained for other HS Schiff base complexes, in agreement with magnetic properties (see below). The higher size of Cl_2An^{2-} ligand compared to the oxalate one gives rise to important differences in the packing of the spin-crossover cation compared to that observed in 2D oxalate-based compounds. Thus, in contrast to oxalate-based compounds, the spin-crossover cations are well isolated from each other as there are not intermolecular contacts between $[Fe^{III}(sal_2\text{-trien})]^+$ complexes belonging to the same layer. This is due to the fact that the size of the hexagons in the anilate-based layers is twice that of the oxalate-based ones. On the contrary, the $[Fe^{III}(sal_2\text{-trien})]^+$ complexes present numerous intermolecular interactions with the anilate-based network and solvent molecules. In particular, they present $\pi-\pi$ stacking interactions between phenolate groups from $[Fe^{III}(sal_2\text{-trien})]^+$ complexes and the anilate ligands of the two neighboring layers. Thus, the two phenolate groups from $[Fe^{III}(sal_2\text{-trien})]^+$ complexes lie parallel to a Cl_2An^{2-} ligand of the upper and lower layer and present short C−C intermolecular distances (distance between the centroids of the two rings 3.475 Å). Furthermore, they present short contacts between their NH groups and Cl and O atoms from the upper and lower anilate-based layers (Figure S3 in the SI).

Structure of $[Fe^{III}(4\text{-OH-sal}_2\text{-trien})][Mn^{II}Cr^{III}(Cl_2An)_3]\cdot$(solvate) (2). This compound crystallizes in the hexagonal chiral space group $P6_122$. The structure is formed by bimetallic anionic sheets in the *ab* plane alternating along the *c* direction with layers containing $[Fe^{III}(4\text{-OH-sal}_2\text{-trien})]^+$ complexes and disordered solvent molecules (Figure 3).

The anionic layer presents the hexagonal honeycomb layer of the previous compound. There is one crystallographically independent Mn(II) and Cr(III), which are localized and distinguishable (M-O bond lengths 2.122(11)-2.221(11) and 1.929(11)-2.035(12) Å, respectively). Mn and Cr present an

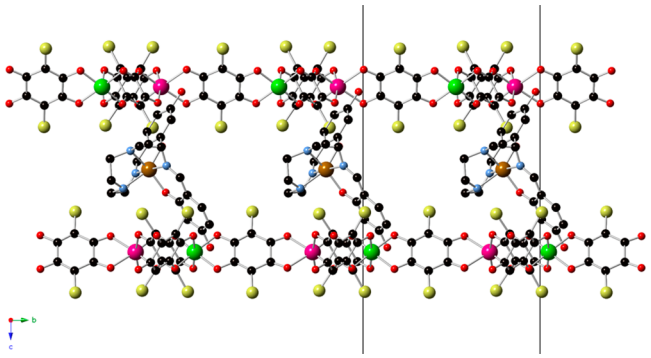

Figure 3. Projection of **2** in the *bc* plane. (Fe (brown), Cr (green), Mn (pink), C (black), N (blue), O (red), Cl (yellow)). Hydrogen atoms have been omitted for clarity.

occupancy of 0.5 as they are in a special position (2-fold axis). As shown in **1**, the configuration of each metal ion is preserved in the neighboring anilate layers. Thus, in the crystal used to solve the structure all the Cr^{III} ions adopt a Δ-configuration, whereas all the Mn^{II} ions adopt the Λ-one. $[Fe^{III}(4\text{-OH-sal}_2\text{-trien})]^+$ complex placed between the anilate layers adopts a Λ-configuration and interacts through several short contacts (see below) with two $\{Cr(Cl_2An)_3\}$ units from the upper and lower neighboring layers, which adopt the opposite configuration (Figure S4 in the SI). The minimum distance between metals of different layers is 11.060 Å, which is similar to that of compounds **1**, **3**, and **4**. As observed in **1**, the anilate-based layers in **2** are alternated.

The cationic layer intercalated between these anilate layers is formed by a crystallographically independent $[Fe^{III}(4\text{-OH-sal}_2\text{-trien})]^+$ complex with an occupancy of 0.5 due to the presence of a 2-fold axis, which runs from the Fe atom to a point placed in the middle of the central ethylene arm of the complex, and disordered solvent molecules. Average Fe−N and Fe−O bond lengths are 2.143(13) and 1.939(13) Å. These values are in the range of those obtained for other HS Schiff base complexes.[12] This contrasts with the LS state found in the $[Fe^{III}(4\text{-OH-sal}_2\text{-trien})]ClO_4$ precursor in the temperature range of 2−300 K.[16] These complexes lie with their long axis almost perpendicular to the anilate network. As in **1**, the two phenolate groups lie parallel to a Cl_2An^{2-} ligand of the upper and lower layers with short C−C intermolecular distances (distance between the centroids of the two rings 3.440 Å) (Figure S4 in the SI). Furthermore, they present short contacts between their NH groups and Cl and O atoms from the upper and lower anilate-based layers. The generalized coordinate calculated with the SHAPE[23] program is around 50%. This indicates that the geometry of the $[Fe^{III}(4\text{-OH-sal}_2\text{-trien})]^+$ complexes is intermediate between a trigonal prism and an octahedron as in **1**, confirming that the intermolecular interactions of these cations with two anilate layers may be the cause of the large distortion of the octahedral geometry. $[Fe^{III}(4\text{-OH-sal}_2\text{-trien})]^+$ complexes belonging to the same layer do not present intermolecular contacts, but interestingly and in contrast to compounds **1**, **3**, and **4**, they form hydrogen-bonds with two $[Fe^{III}(4\text{-OH-sal}_2\text{-trien})]^+$ complexes of neighboring layers. This is a consequence of the large size of the hexagonal channels of the anilate-based anionic network that allows a high degree of penetration of the inserted cation. The lateral view of the structure (Figure 4) shows that the hydroxy groups from $[Fe^{III}(4\text{-OH-sal}_2\text{-trien})]^+$ complexes penetrate the anilate-based

dx.doi.org/10.1021/ic5016803 | *Inorg. Chem.* 2014, 53, 12014−12026

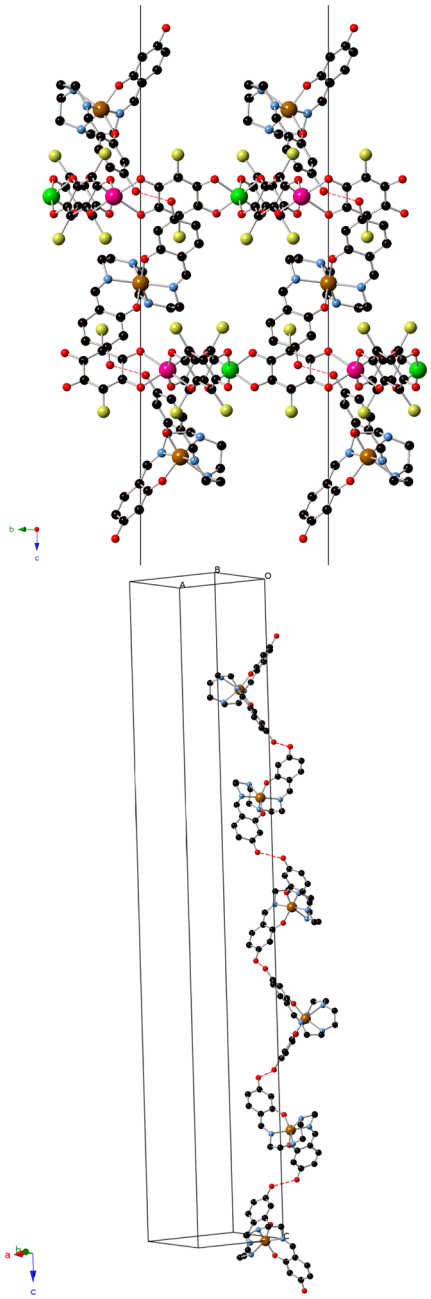

Figure 4. Projection of **2** in the *bc* plane showing the hydrogen bonds between $[Fe^{III}(4\text{-OH-sal}_2\text{-trien})]^+$ complexes from different layers (up). Helical chain of $[Fe^{III}(4\text{-OH-sal}_2\text{-trien})]^+$ complexes from different layers linked through hydrogen bonds (red dashed lines) (down). (Fe (brown), Cr (green), Mn (pink), C (black), N (blue), O (red), Cl (yellow)). Hydrogen atoms have been omitted for clarity.

network, allowing the formation of hydrogen bonds with the $[Fe^{III}(4\text{-OH-sal}_2\text{-trien})]^+$ complexes from the upper and lower cationic layers. This gives rise to helical chains of $[Fe^{III}(4\text{-OH-sal}_2\text{-trien})]^+$ complexes (Figure 4) linked through hydrogen-bond interactions running along the *c* axis. This type of interactions has never been found in oxalate-based compounds. Finally, another consequence of the larger size of X_2An^{2-} ligands compared to the oxalate ones is the presence of holes in the structure surrounding the $[Fe^{III}(4\text{-OH-sal}_2\text{-trien})]^+$ complexes that are occupied by disordered solvent molecules and that could not be modeled (see Experimental Section and cif files). Indeed, crystals of **2** lose solvent very quickly when they are extracted from their mother liquor. Projection of the structure along the *bc* plane shows the presence of channels along the *a* axis that could be filled with different guest molecules (Figure 3). Thus, these compounds present a void volume of ca. 5383 $Å^3$ (ca. 50% of the unit cell volume), where solvent molecules could be absorbed, opening the way to the synthesis of new porous magnets.

Structure of $[Fe^{III}(sal_2\text{-epe})][Mn^{II}Cr^{III}(Br_2An)_3]\cdot(CH_3CN_4\cdot$ (solvate) (3) and $[Fe^{III}(5\text{-Cl-sal}_2\text{-trien})][Mn^{II}Cr^{III}(Br_2An)_3]\cdot(CH_2Cl_2)\cdot(CH_3OH)\cdot(H_2O)_4\cdot(CH_3CN)_{1.5}\cdot$(solvate) (4). The two compounds crystallize in the monoclinic space group $P2_1/c$. Their structure consists of 2D bimetallic $[MnCr(Br_2An)_3]^-$ layers in the *ab* plane with a honeycomb structure similar to that observed in compounds **1** and **2**, alternating with $[Fe^{III}(sal_2\text{-epe})]^+$ (in **3**) or $[Fe^{III}(5\text{-Cl-sal}_2\text{-trien})]^+$ (in **4**) cations and solvent molecules (Figure 5).

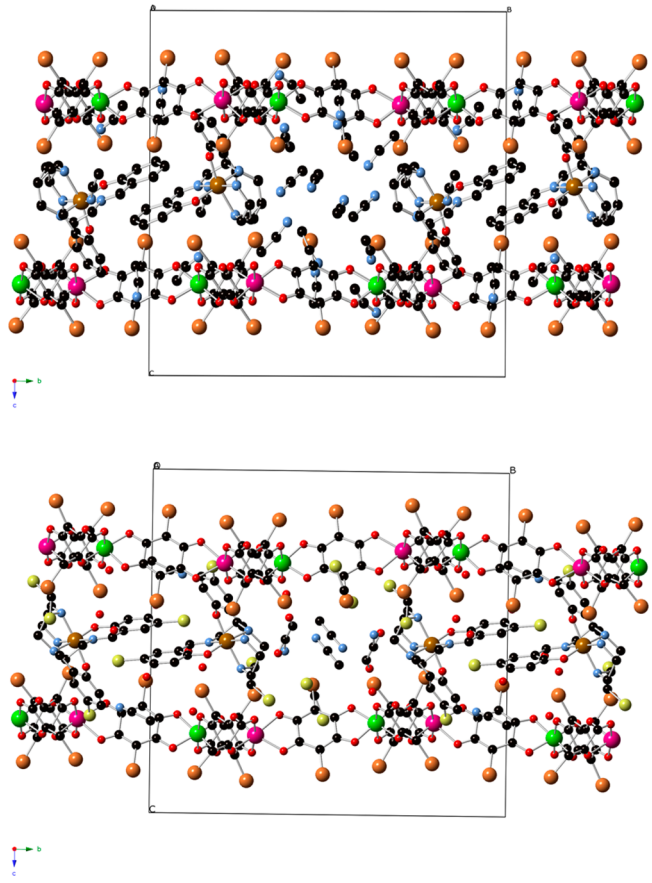

Figure 5. Projections of **3** (up) and **4** (down) in the *bc* plane. (Fe (brown), Br (orange), Cr (green), Mn (pink), C (black), N (blue), O (red), Cl (yellow)). Hydrogen atoms have been omitted for clarity.

In **4**, there is one crystallographically independent Mn(II) and Cr(III), which are localized and distinguishable (M−O bond lengths of 2.126(13)−2.206(16) Å and 1.961(15)−2.000(15) Å, respectively). Due to the presence of an inversion center located between the anilate-based layers, Mn and Cr ions from consecutive layers present opposite configurations. In contrast, the M−O bond lengths of the two crystallographically independent metal atoms of the anilate-based network in **3** (in the range of 2.007(16)−2.127(15) Å) are intermediate between those expected for Mn−O and Cr−O bonds indicating a higher

dx.doi.org/10.1021/ic5016803 | *Inorg. Chem.* 2014, 53, 12014−12026

degree of disorder. The minimum distance between metals of different layers is 11.919 Å for **3** and 11.557 Å for **4**, similar to those observed in compounds **1** and **2**. The anilate-based layers in **3** and **4** are also alternated.

The $[Fe^{III}(sal_2\text{-epe})]^+$, or $[Fe^{III}(5\text{-Cl-sal}_2\text{-trien})]^+$ complexes, and disordered solvent molecules occupying the space between the layers present a different packing to that shown in compounds **1** and **2**. Thus, two neighboring Fe(III) complexes present several intermolecular interactions that involve the two phenolate rings ($\pi-\pi$ stacking interactions between the two aromatic rings and two C−H···π or C−Cl···π interactions). These dimers of $[Fe^{III}(sal_2\text{-epe})]^+$ or $[Fe^{III}(5\text{-Cl-sal}_2\text{-trien})]^+$ complexes are well isolated from other Fe(III) complexes, although they present numerous intermolecular interactions with solvent molecules and with the anilate-based layers. In contrast to **1** and **2**, only one of the two phenolate groups of the cations present $\pi-\pi$ stacking interactions with the Br_2An^{2-} groups from the anilate-based layer as the other one is involved in the intermolecular interactions with a neighboring $[Fe^{III}(sal_2\text{-epe})]^+$ or $[Fe^{III}(5\text{-Cl-sal}_2\text{-trien})]^+$ complex as mentioned above (Figure S5 in the SI). $[Fe^{III}(sal_2\text{-epe})]^+$ and $[Fe^{III}(5\text{-Cl-sal}_2\text{-trien})]^+$ complexes present a distorted octahedral geometry with average Fe−N and Fe−O bond lengths of 2.122(18) and 1.939(16) Å for **3** and 1.98(2) and 1.854(18) Å for **4**. These bond lenghts indicate that the Fe ions in **3** are in the HS state, whereas those in **4** are in the LS one, in agreement with magnetic measurements (see below). SHAPE calculations[23] show that the coordination geometry around the Fe ion in **3** and **4** is closer to a perfect octahedron than that of compounds **1** and **2** (the generalized coordinate between a perfect octahedron and a perfect trigonal prism is 30.3% for **3** and 14.3% for **4**). These values are similar to those reported for similar complexes inserted into oxalate-based networks taking into account that HS complexes, as those of **3**, normally present a higher trigonal distortion.[12h] The higher trigonal distortion of **1** and **2** (with generalized coordinates of ca. 50%) may be related to the distortions generated by the $\pi-\pi$ intermolecular interactions between the Fe(III) complexes and two anilate rings of two neighboring layers. Finally, the structures of **3** and **4** present numerous voids that are occupied by disordered solvents. Some of them could not be modeled (see Experimental Section and cif files). Indeed, crystals of **3** and **4** lose solvent very quickly when they are out of the mother liquor.

Structure of $[Fe^{II}(tren(imid)_3)]_2[Mn^{II}Cl_2Cr^{III}(Cl_2An)_3]Cl\cdot(CH_3OH)\cdot(CH_2Cl_2)_3\cdot(CH_3CN)_{0.5}$ (5). This compound crystallizes in the triclinic space group *P*-1. It is formed by anionic $[Mn^{II}Cl_2Cr^{III}(Cl_2An)_3]^{3-}$ chains running along the *a* axis surrounded by $[Fe^{II}(tren(imid)_3)]^{2+}$, Cl^-, and solvent molecules (acetonitrile, methanol, or dichloromethane). These bimetallic anionic chains contain one crystallographically independent Cr and Mn with characteristic Mn−O and Cr−O distances (2.164(4)−2.370(4) Å for Mn1 and 1.950(4)−1.993(4) Å for Cr1). Furthermore, Mn is linked to two Cl^- anions in cis at 2.3823(19) and 2.4258(19) Å. These chains are formed by $[Cr^{III}(Cl_2An)_3]^{3-}$ complexes bonded to two Mn(II) ions through two bis-bidentate chloranilate bridges while the third chloranilate is a terminal one (see Figure 6). At the same time, the Mn(II) ions are coordinated to two chelating bis(bidentate) chloranilate bridges from two neighboring $[Cr^{III}(Cl_2An)_3]^{3-}$ complexes and to two chloride ion in cis (see Figure 6). These chains are formed by Mn and Cr ions of opposite chirality building a zigzag alternating arrangement of

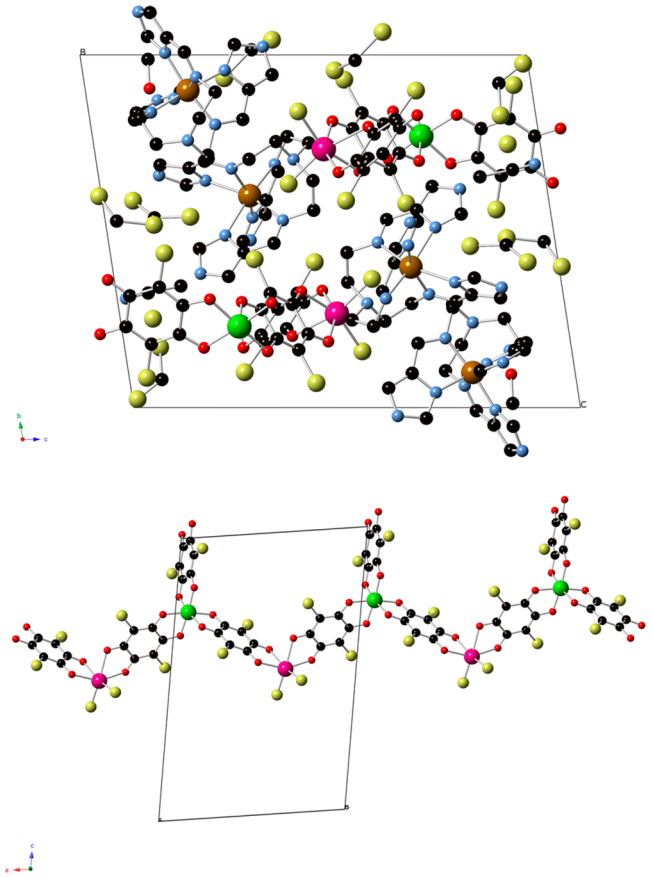

Figure 6. Projection of **5** in the *bc* plane (up). $[Mn^{II}Cl_2Cr^{III}(Cl_2An)_3]^{3-}$ chains in the structure of **5** (down). (Fe (brown), Cr (green), Mn (pink), C (black), N (blue), O (red), Cl (yellow)). Hydrogen atoms have been omitted for clarity.

complexes. Due to the centrosymmetric space group, chains of both chiralities are observed in the structure related by an inversion center. $[Fe^{II}(tren(imid)_3)]^{2+}$ complexes, Cl^- anions, and solvent molecules surround these chains (Figure 6). $[Mn^{II}Cl_2Cr^{III}(Cl_2An)_3]^{3-}$ chains are in close contact with a neighboring one through halogen−halogen interactions[24] involving a Cl atom from Cl_2An ligand (Cl1) with minimum Cl···Cl interchain distances of 3.130 Å (Figure S6 in the SI). The shortest distance between metals of neighboring chains is 8.445 Å. These chains present numerous short contacts with free Cl^- anions, $[Fe^{II}(tren(imid)_3)]^{2+}$ complexes, and solvent molecules.

$[Fe^{II}(tren(imid)_3)]^{2+}$ complexes, Cl^- anions, and solvent molecules are intercalated in the holes between these chains. There are two crystallographically independent $[Fe^{II}(tren(imid)_3)]^{2+}$ complexes in which Fe exhibits a distorted octahedral coordination environment involving six N donor atoms of the hexadentate Schiff base: three Fe−N(imine) and three Fe−N(imidazolyl) bonds. The average Fe−N distances of the two complexes (1.988(6) Å for the complex with Fe1 and 2.213(5) Å for the complex with Fe2) are close to the ones expected for LS (Fe1) and HS (Fe2).[17] These distances indicate that at 120 K, the temperature of the structural resolution, half of the Fe(II) complexes are in the HS state in agreement with magnetic measurements of the dry samples, see below. On the other hand, average Fe−N distances of the two complexes in the structure of another crystal solved at 220 K (2.162(10) Å for the complex with Fe1 and 2.235(8) Å for the

dx.doi.org/10.1021/ic5016803 | *Inorg. Chem.* 2014, 53, 12014−12026

complex with Fe2) are close to the expected ones for HS Fe(II). Furthermore, changes in the unit cell of this crystal indicate a shortening of *b* axis from 220 to 120 K, whereas the *a* and *c* axes remain almost constant (Figure S7 in the SI). At the same time, the unit cell volume decreases gradually from 220 to 120 K. All these changes are more important in the spin-crossover region (see below) from 220 to 140 K, indicating that they are associated with the change of spin state of half of the $[Fe^{II}(tren(imid)_3)]^{2+}$ complexes. It was not possible to solve the structure at 300 K due to the loss of crystallinity.

NH groups from two of the three imidazole ligands linked to Fe1 form hydrogen bonds with the Cl^- anion and a methanol molecule. In the same way, two of the three NH groups of $tren(imid)_3$ linked to Fe2 form hydrogen bonds with the two oxygens of the terminal chloranilate ligand of Cr and the Cl^- anion. These hydrogen bonds between a terminal Cl_2An ligand and the NH groups of $[Fe^{II}(tren(imid)_3)]^{2+}$ could explain the coexistence of terminal and bridging Cl_2An ligands in this structure as they may compete with the coordination to a metal. This has also been observed in the bimetallic oxalate-based compounds obtained with $[Fe^{II}(tren(imid)_3)]^{2+}$.[12g] Cl^- anions occupy the holes between the $[Fe^{II}(tren(imid)_3)]^{2+}$ cations. As mentioned above, they form two hydrogen bonds with NH groups from two neighboring $[Fe^{II}(tren(imid)_3)]^{2+}$ complexes.

Finally, there are numerous holes that are occupied by acetonitrile, methanol, and dichloromethane solvent molecules, which are disordered in some cases.

Magnetic Properties. Magnetic properties of **2** were measured for crystals of this compound in contact with the mother liquor to avoid the fast loss of solvent molecules. The magnetic properties of the other four compounds were measured in freshly filtered samples. The product of the molar magnetic susceptibility times the temperature ($\chi_m T$) of the four 2D compounds is shown in Figure 7. It presents at 300 K a value close to 11.1 cm^3 K mol^{-1} for **1**, **2**, and **3**, and 8.3 cm^3 K mol^{-1} for **4**. These values are close to the expected ones for noninteracting Mn(II) and Cr(III) plus the contribution of a HS Fe(III) ion (10.6 cm^3 K mol^{-1} for $g = 2$) in the case of **1**, **2**, and **3**, although the lower value found in **4** indicates that most of the Fe(III) are in the LS state (expected value around 6.8 cm^3 K mol^{-1}). When the temperature is lowered, $\chi_m T$ of the four compounds shows a continuous decrease reaching a minimum value at 19.2 K (8.0 cm^3 K mol^{-1}) for **1**, 24.0 K (8.5 cm^3 K mol^{-1}) for **2**, 20.0 K (8.1 cm^3 K mol^{-1}) for **3**, and 18.5 K (5.9 cm^3 K mol^{-1}) for **4** followed by a sharp increase at lower temperatures with maxima between 6 and 9 K. The decrease of $\chi_m T$ with the temperature may be attributed to antiferromagnetic Mn−Cr interactions mediated through the X_2An^{2-} bridges, as observed in $[NBu_4]^+$ and $[(H_3O)(phz)_3]^+$ salts containing similar $[Mn^{II}Cr^{III}(X_2An)_3]^-$ layers (X = Cl, Br, I and H).[14a] Because the ground spin states of Cr^{III} and Mn^{II} are different (3/2 and 5/2, respectively), this interaction leads to an antiferromagnetic coupling that results in a $\chi_m T$ minimum, followed by an increase of $\chi_m T$ below ca. 18−22 K, and finally by a ferrimagnetic long-range ordering at low temperatures for the four compounds. Furthermore, structural data may help to understand the contribution of the spin crossover to the observed decrease of $\chi_m T$. Thus, as the Fe−N and Fe−O bond lenghts of **1**, **2**, and **3** at 120 K indicate that the Fe(III) ions are HS at this temperature, we conclude that only a small fraction of Fe(III) ions in **1**, **2**, and **3** undergo spin crossover from 300 to 120 K. An additional proof of the absence of a significant spin-crossover transition in these three compounds is the linear behavior of the χ_m^{-1} versus T curve in the 50−300 K temperature range. This plot can be fitted to a Curie−Weiss law ($\chi_m^{-1} = (T - \theta)/C$) leading to Weiss constants, $\theta = -20.0$ K for **1**, $\theta = -15.1$ K for **2**, and $\theta = -13.1$ K for **3**, which are close to those of other 2D $Mn^{II}Cr^{III}$ anilate-based networks.[14a] In the case of compound **4**, Fe−N and Fe−O bond lengths at 120 K indicate that the Fe(III) complex is predominantly LS at this temperature. Therefore, the $\chi_m T$ value of **4** at 300 K and the approximately constant difference of $\chi_m T$ of **1**, **2**, and **3** with respect to that of **4**, indicate that most of the Fe(III) ions of this compound are in the LS state from 300 to 120 K. An additional proof of the absence of a significant spin crossover in **4** is the linear behavior of the χ_m^{-1} versus T curve in the 50−300 K temperature range (θ value of −13.5 K). Mössbauer measurements are needed to confirm the LS/HS Fe(III) ratios of these compounds with the temperature, but they could not be performed due to the small amount of sample available.

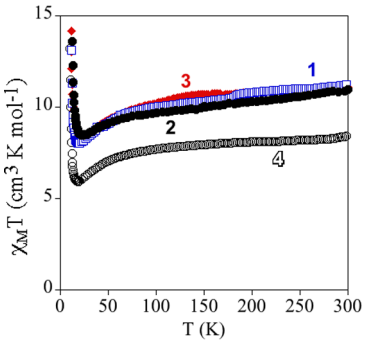

Figure 7. Temperature dependence of the product of the molar magnetic susceptibility times the temperature ($\chi_m T$) of **1** (empty blue squares), **2** (full circles), **3** (full red diamonds), and **4** (empty circles) with an applied field of 0.1 mT.

The confirmation of the long-range order and a more accurate determination of the ordering temperatures can be obtained from the susceptibility measurements performed with an alternating magnetic field (AC susceptibility). These measurements show a frequency-independent peak in the in-phase molar susceptibility (χ_m') and out-of-phase molar susceptibility (χ_m'') of the four 2D compounds (Figure 8). In the case of **1**, the χ_m'' is very weak and only appears at the lowest frequencies (1 and 10 Hz). On the contrary, **2**, **3**, and **4** show clear frequency-independent peaks in χ_m' and χ_m'' (Figure 8). In some cases, secondary peaks appear at lower temperatures that could be explained by formation of magnetic domains and domain-wall movement, as in the oxalate-based networks.[12] The ordering temperature, T_c, determined as the temperature at which χ_m'' becomes nonzero is ca. 10 K for **1**, 10.4 K for **2**, 10.2 K for **3**, and 9.8 K for **4**. These T_c values are much higher than those found for the $[NBu_4]^+$ and $[(H_3O)(phz)_3]^+$ salts containing similar $[Mn^{II}Cr^{III}(Cl_2An)_3]^-$ or $[Mn^{II}Cr^{III}(Br_2An)_3]^-$ layers (5.5 and 6.3 K),[14a] in contrast to oxalate-based 2D compounds, where T_c remains constant for a given 2D $[M^{II}M^{III}(C_2O_4)_3]^-$ lattice, independently of the inserted cation. We can, therefore, conclude that the magnetic coupling and, accordingly, the ordering temperatures of these heterometallic 2D anilate-based networks are much more sensitive to the changes of the inserted cations than the corresponding oxalate ones. The possible reasons to explain this effect are the presence of intermolecular interactions between the anilate ligands and Fe(III) complexes (π−π

dx.doi.org/10.1021/ic5016803 | Inorg. Chem. 2014, 53, 12014−12026

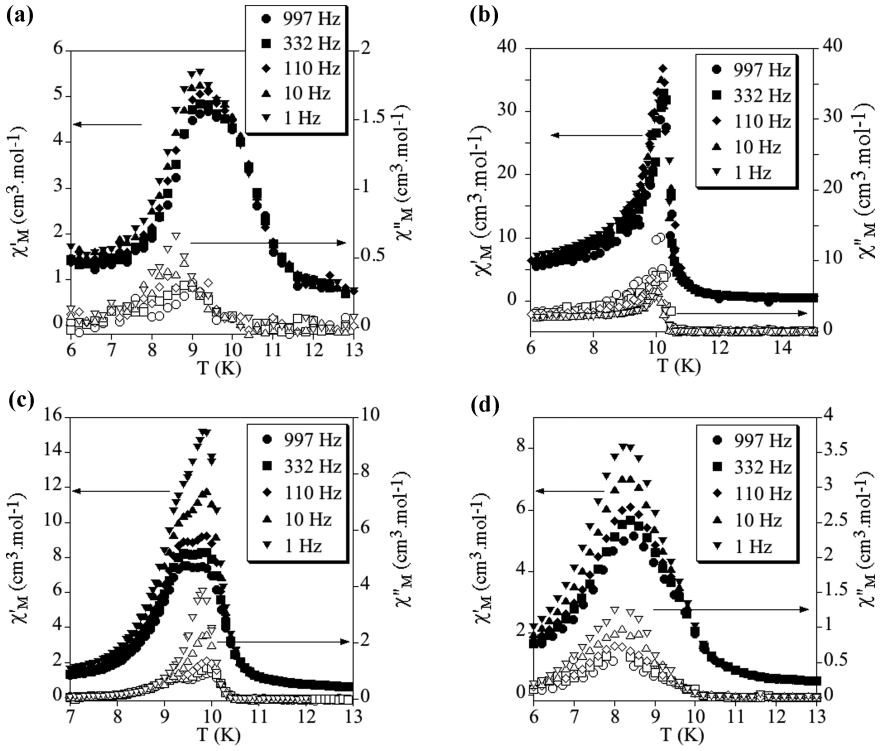

Figure 8. Temperature dependence of the in-phase AC susceptibility (χ') (filled symbols) and the out-of-phase AC susceptibility (χ'') of **1** (a), **2** (b), **3** (c), and **4** (c).

interactions and NH···O and NH···Cl/Br interactions mentioned above), which are not observed in $[NBu_4]^+$ and $[(H_3O)(phz)_3]^+$ salts containing similar $[Mn^{II}Cr^{III}(Cl_2An)_3]^-$ or $[Mn^{II}Cr^{III}(Br_2An)_3]^-$ layers. Some of these interactions could result in an increase of the Mn(II)−Cr(III) coupling constant through the anilate ligand and, accordingly, of T_c. In fact, these exchange interactions have shown to be very sensitive to small electronic changes introduced in the anilate bridge. Thus, in the series $(NBu_4)[Mn^{II}Cr^{III}(X_2An)_3]$, a change in the electron density in the anilate ring by changing X from Cl to H has resulted in an increase of T_c from 5.5 K up to 11.0 K.[14a] Interestingly, this modulation of T_c with the inserted cation (or even with solvent molecules), besides the already observed modulation with X,[14a] represents an additional advantage of the anilate-based networks compared with the oxalate ones.

The ferrimagnetic nature of the long-range ordering is confirmed by the isothermal magnetization measurements at 2 K that show a sharp increase of the magnetization at low fields that becomes more gradual at higher fields (Figure 9). At low fields (H < 0.2 T), the magnetizations of the four compounds increase with a high slope reaching values in the range 1.4−1.6 μ_B at H = 0.1 T (inset in Figure 9). At higher fields, the magnetization of the four compounds shows a gradual and nonlinear increase, which is higher in the case of **1**, **2**, and **3** (7.1 μ_B for **1**, 6.3 μ_B for **2**, and 7.2 μ_B for **3** at 5 T) than in **4** (4.0 μ_B at 5 T). These values are still far from saturation. The magnetization at lower fields is close to the expected value for a ferrimagnetic $Mn^{II}Cr^{III}$ network (M_s = 5 μ_B − 3 μ_B = 2 μ_B, possibly reduced by spin-canting effects in the anilate network). The gradual nonlinear increase observed at higher fields may be due to the contribution of the paramagnetic Fe(III) plus the result of the competition between the antiferromagnetic couplings and the Zeeman interaction with the external

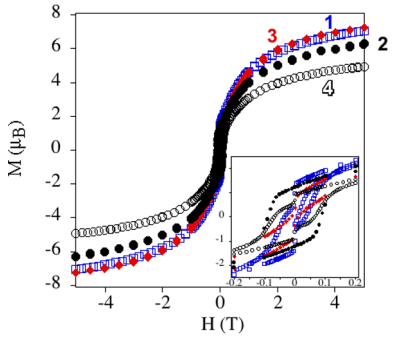

Figure 9. Isothermal magnetization at 2 K of **1** (empty blue squares), **2** (full circles), **3** (full red diamonds), and **4** (empty circles).

magnetic field. The higher increase in **1**, **2**, and **3** compared to that in **4** indicates that most of the Fe(III) of **1**, **2**, and **3** are in the HS state, whereas those of **4** are in the LS state at **2** K, in agreement with susceptibility measurements. These isothermal magnetization measurements also provide an additional proof of the magnetic ordering exhibited by these compounds because they present hysteresis below the ordering temperatures with coercive fields of ca. 35 mT for **1**, 87 mT for **2**, 10 mT for **3**, and 66 mT for **4** (Figure 9).

The χ_mT of **5** is shown in Figure 10. It presents at 300 K a value of 11.2 cm^3 K mol^{-1}. This value is close to the expected one for noninteracting Mn(II) and Cr(III) plus the contribution of two HS Fe(II) ion (12.25 cm^3 K mol^{-1} for g = 2) in agreement with crystal structure at 220 K, which suggests that most of the Fe(II) are in the HS. From 280 to 100 K, χ_mT shows a continuous decrease reaching a value of 8.4 cm^3 K mol^{-1} at 100 K. The decrease of χ_mT in this range of temperature (~3 cm^3 K mol^{-1}) corresponds to the expected one for the spin crossover of half of the Fe(II). This is

dx.doi.org/10.1021/ic5016803 | Inorg. Chem. 2014, 53, 12014−12026

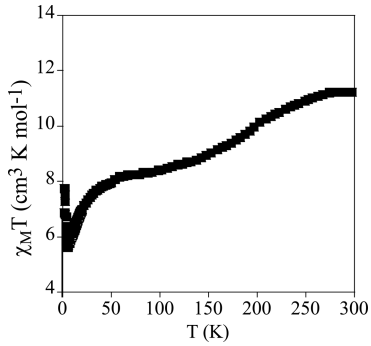

Figure 10. Temperature dependence of the product of the molar magnetic susceptibility times the temperature ($\chi_m T$) of **5** with an applied field of 0.1 mT.

supported by the structural data at 120 K, which indicate that 50% of Fe(II) are in the HS at this temperature (see above). At lower temperatures, $\chi_m T$ presents a gradual decrease that becomes very abrupt below 50 K to reach a minimum at 4.8 K followed by a sharp increase at lower temperatures. This behavior may be attributed to the antiferromagnetic Mn−Cr interactions mediated through the X_2An^{2-} bridges within the chains, as observed in the other compounds in this paper. This is supported by the magnetic data of other Mn^{II}−Cr^{III} chains of similar structure to that of **5** with diamagnetic counterions, obtained very recently by us, that show a very gradual decrease of $\chi_m T$ from 300 K (6.3 cm^3 K mol^{-1}) to 100 K (6.1 cm^3 K mol^{-1}) and an abrupt decrease below 50 K with a minimum at 6 K (2.5 cm^3 K mol^{-1}) followed by a sharp increase at lower temperatures.[25]

AC measurements show a frequency-independent peak in χ_m' and χ_m'' at temperatures below 2.6 K (Figure 11). This

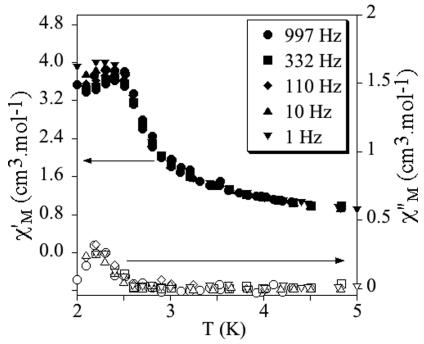

Figure 11. Temperature dependence of the in-phase AC susceptibility (χ') (filled symbols) and the out-of-phase AC susceptibility (χ'') of **5**.

indicates that the compound presents a magnetic long-range ordering below this temperature. The lack of frequency dependence of the AC peaks excludes a single- chain magnet (SCM) behavior.

The ferrimagnetic nature of the long-range ordering is confirmed by the isothermal magnetization measurements at 2 K that show a sharp increase of the magnetization at low fields (1.5 μ_B at H = 0.2 T) that becomes more gradual at higher fields (Figure S8 in the SI). As in the four previous compounds, the magnetization at lower fields is close to the expected value for a ferrimagnetic $Mn^{II}Cr^{III}$ network ($M = 5\,\mu_B - 3\,\mu_B = 2\,\mu_B$), while the gradual nonlinear increase observed at higher fields may be due to the contribution of the paramagnetic HS Fe(II). The hysteresis loop does not show a measurable coercive field. Therefore, this compound behaves as a soft magnet. The magnetic ordering must be the result of the ferromagnetic interchain interactions, induced by dipolar interactions and also by a possible superexchange pathway that can work through the halogen−halogen interchain interactions (see above). The synthesis of other compounds with a similar structure (replacement of $[Fe^{II}(tren(imid)_3)]^{2+}$ by diamagnetic complexes or of Cl_2An by Br_2An) is in progress in order to understand the role played by spin-crossover complexes and X_2An ligands in the interchain interactions.

CONCLUSION

Five novel compounds formed by $[Fe^{III}(sal_2\text{-trien})]^+$, $[Fe^{III}(5\text{-Cl-sal}_2\text{-trien})]^+$, $[Fe^{III}(sal_2\text{-epe})]^+$, $[Fe^{III}(4\text{-OH-sal}_2\text{-trien})]^+$, and $[Fe^{II}(tren(imid)_3)]^{2+}$ and anionic bimetallic coordination polymers based on the anilate ligand have been prepared and characterized. Two-dimensional anilate-based networks with a honeycomb structure have been obtained with the $[Fe^{III}(sal_2\text{-trien})]^+$ complex and derivatives (compounds **1**−**4**), whereas a one-dimensional (1D) anilate-based network has been obtained with $[Fe^{II}(tren(imid)_3)]^{2+}$ (compound **5**).

The first consequence of the replacement of oxalate by anilate ligands for $[Fe^{III}(sal_2\text{-trien})]^+$ and derivatives is that the formation of 2D compounds is favored when the larger anilate ligands are used. With oxalate ligands, one obtains either 2D or 3D networks, depending on the substituent of sal_2-trien. A second consequence is that, due to the larger size of anilate ligands, the distances between the Fe(III) complexes inserted between the anilate-layers are larger. This leads in some cases to the absence of intermolecular interactions between the spin-crossover complexes belonging to the same layer (**1** and **2**) or to the presence of isolated dimers of Fe(III) complexes (**3** and **4**). Furthermore, this results in the presence of large voids filled with disordered solvent molecules. Finally, a third consequence of the substitution of oxalate by anilate is the presence of π−π stacking interactions between the anilate ligands and the phenolate rings of the spin-crossover complexes, which is not observed in the oxalate-based compounds. These π−π interactions, more important in compounds **1** and **2**, lead to a larger trigonal distortion of the octahedral geometry of Fe(III) in these compounds. The rigidity imposed by π−π stacking with the anilate ligands and the lack of intermolecular interactions between the Fe(III) complexes may be at the origin of the absence of a significant spin crossover in the 2D compounds. Thus, the magnetic properties indicate that most of the inserted Fe(III) cations remain in their HS (**1**, **2**, and **3**) or LS state (**4**). At the same time the anilate network presents a ferrimagnetic ordering at ca. 10 K, which is significantly higher than the ordering temperatures obtained for oxalate networks with the same metal ions (ca. 5 K) or for 2D anilate networks with other templating cations (ca. 6 K for $[NBu_4]^+$ and $[(H_3O)(phz)_3]^+$ salts). Notice that the presence of pores in these structures and the chiral character of some of them could lead to new functionalities, in addition to the magnetic ordering such as solvent adsorption, proton conduction or chirality.

The preparation of anilate-based compounds combining spin crossover and magnetic ordering has been achieved with the use of $[Fe^{II}(tren(imid)_3)]^{2+}$ complex, which do not present spin crossover in bimetallic oxalate-based compounds.[12g] Compound **5** presents a 1D anionic anilate-based network surrounded by $[Fe^{II}(tren(imid)_3)]^{2+}$ complexes, Cl^- anions, and solvent molecules. The main difference with the previous

dx.doi.org/10.1021/ic5016803 | Inorg. Chem. 2014, 53, 12014−12026

series of 2D compounds is that the spin-crossover complexes do not show $\pi-\pi$ stacking interactions with the anilate ligands and present numerous intermolecular contacts among them. As a result of this, **5** shows coexistence of spin crossover of half of the Fe(II) complexes from 280 to 100 K and a ferrimagnetic coupling within the chains that gives rise to a magnetic ordering below 2.6 K. Photomagnetic measurements are in progress to study the possible effect of a photoinduced spin crossover in the magnetic properties of the anilate-based network in the search for a magnetic responsive material.

Finally, an additional advantage provided by this type of networks that remains to be explored is the functionalization of the anilate ligands with substituents leading to strong intermolecular interactions between the ferrimagnetic network and the spin-crossover complex or even covalent bonding between the two networks in order to enhance the interactions between them and to improve their responsive character.

■ ASSOCIATED CONTENT

Supporting Information

Structural views of **1**, **2**, **3**, **4**, and **5**. Changes of the unit cell parameters with the temperature and isothermal magnetization of **5** at 2 K. This material is available free of charge via the Internet at http://pubs.acs.org.

■ AUTHOR INFORMATION

Corresponding Authors

*E-mail: miguel.clemente@uv.es. Fax: (+34) 96 354 3273. Tel: (+34) 96 3544415.

*E-mail: eugenio.Coronado@uv.es.

Notes

The authors declare no competing financial interest.

■ ACKNOWLEDGMENTS

We thank the EU (SPINMOL ERC Adv. Grant), the Spanish MINECO (CTQ-2011-26507, and MAT2011-22785) and the Generalitat Valenciana (Prometeo and ISIC-Nano programs) for financial support. The authors also thank J. M. Martínez-Agudo and Dr. G. Agustí-López, University of Valencia, for magnetic characterization.

■ REFERENCES

(1) (a) Coronado, E.; Day, P. *Chem. Rev.* **2004**, *104*, 5419−5448. (b) Coronado, E.; Martí- Gastaldo, C.; Navarro-Moratalla, E.; Ribera, A.; Blundell, S. J.; Baker, P. J. *Nat. Chem.* **2010**, *2*, 1031−1036. (c) Coronado, E.; Martí-Gastaldo, C.; Navarro-Moratalla, E.; Burzuri, E.; Camon, E.; Luis, F. *Adv. Mater.* **2011**, *23*, 5021−5026. (d) Bourzami, R.; Eyele-Mezui, S.; Delahaye, E.; Drillon, M.; Rabu, P.; Parizel, N.; Choua, S.; Turek, P.; Rogez, G. *Inorg. Chem.* **2014**, *53*, 1184−1194.

(2) Coronado, E.; Mínguez Espallargas, G. *Chem. Soc. Rev.* **2013**, *42*, 1525−1539.

(3) See for general reviews: (a) Spin Crossover in Transition Metal Compounds. *Topics in Current Chemistry*; Gütlich, P., Goodwin, H. A., Eds.; Springer Verlag: Berlin-Heidelberg- New York, 2004; Vols. *233*−*235*. (b) *Spin-Crossover Materials: Properties and Applications*; Halcrow, M. A., Ed.; Wiley: New York, 2013.

(4) Clemente-León, M.; Coronado, E.; Martí-Gastaldo, C.; Romero, F. M. *Chem. Soc. Rev.* **2011**, *40*, 473−497.

(5) (a) Clemente-León, M.; Galán-Mascarós, J. R.; Gómez-García, C. J. *Chem. Commun.* **1997**, 1727−1728. (b) Coronado, E.; Galán-Mascarós, J. R.; Gómez-García, C. J.; Martínez-Agudo, J. M. *Adv. Mater.* **1999**, *11*, 558−561. (c) Coronado, E.; Galán-Mascarós, J. R.; Gómez-García, C. J.; Ensling, J.; Gutlich. *Chem.—Eur. J.* **2000**, *6*, 552−563.

(6) (a) Bénard, S.; Yu, P.; Audière, J. P.; Rivière, E.; Clèment, R.; Ghilhem, J.; Tchertanov, L.; Nakatami, K. *J. Am. Chem. Soc.* **2000**, *122*, 9444−9454. (b) Aldoshin, S. M.; Sanina, N. A.; Minkin, V. I.; Voloshin, N. A.; Ikorskii, V. N.; Ovcharenko, V. I.; Smirnov, V. A.; Nagaeva, N. K. *J. Mol. Struct.* **2007**, *826*, 69−74.

(7) (a) Coronado, E.; Galán-Mascarós, J. R.; Gómez-García, C. J.; Laukhin, V. *Nature* **2000**, *408*, 447−449. (b) Alberola, A.; Coronado, E.; Galán-Mascarós, J. R.; Giménez-Saiz, C.; Gómez- García, C. J. *J. Am. Chem. Soc.* **2003**, *125*, 10774−10775. (c) Galán-Mascarós, J. R.; Coronado, E.; Goddard, P. A.; Singleton, J.; Coldea, A. I.; Wallis, J. D.; Coles, S. J.; Alberola, A. *J. Am. Chem. Soc.* **2010**, *132*, 9271−9273. (d) Coronado, E.; Galán-Mascarós, J. R.; Gómez-García, C. J.; Martínez-Ferrero, E.; Van Smaalen, S. *Inorg. Chem.* **2004**, *43*, 4808−4810. (e) Zhang, B.; Zhang, Y.; Zhu, D. *Chem. Commun.* **2012**, *48*, 197−199.

(8) (a) Okawa, H.; Shigematsu, A.; Sadakiyo, M.; Miyagawa, T.; Yoneda, K.; Ohba, M.; Kitagawa, H. *J. Am. Chem. Soc.* **2009**, *131*, 13516−13522. (b) Pardo, E.; Train, C.; Contard, G.; Boubekeur, K.; Fabelo, O.; Liu, H.; Dkhil, B.; Lloret, F.; Nakagawa, K.; Tokoro, H.; Ohkoshi, S.-I.; Verdaguer, M. *J. Am. Chem. Soc.* **2011**, *133*, 15328−15331. (c) Sadayiko, M.; Okawa, H.; Shigematsu, A.; Ohba, M.; Yamada, T.; Kitagawa, H. *J. Am. Chem. Soc.* **2012**, *134*, 5472−5475. (d) Okawa, H.; Sadakiyo, M.; Yamada, T.; Maesato, M.; Ohba, M.; Kitagawa, H. *J. Am. Chem. Soc.* **2013**, *135*, 2256−2262.

(9) (a) Endo, T.; Akutagawa, T.; Noro, S. I.; Nakamura, T. *Dalton Trans.* **2011**, *40*, 1491−1496. (b) Pardo, E.; Train, C.; Liu, H.; Chamoreau, L.-M.; Dkhil, B.; Boubekeur, K.; Lloret, F.; Nakatani, K.; Tokoro, H.; Ohkoshi, S.-i.; Verdaguer, M. *Angew. Chem., Int. Ed.* **2012**, *51*, 8356−8360.

(10) (a) Andrés, R.; Gruselle, M.; Malézieux, B.; Verdaguer, M.; Vaissermann, J. *Inorg. Chem.* **1999**, *38*, 4637−4646. (b) Andrés, R.; Brissard, M.; Gruselle, M.; Train, C.; Vaissermann, J.; Malézieux, B.; Jamet, J. P.; Verdaguer, M. *Inorg. Chem.* **2001**, *40*, 4633−4640. (c) Clemente- León, M.; Coronado, E.; Dias, J. C.; Soriano-Portillo, A.; Willett, R. D. *Inorg. Chem.* **2008**, *47*, 6458−6463. (d) Train, C.; Gheorghe, R.; Krstic, V.; Chamoreau, L. M.; Ovanesyan, N. S.; Rikken, G. L. J. A.; Gruselle, M.; Verdaguer, M. *Nat. Mater.* **2008**, *7*, 729−734. (e) Train, C.; Nuida, T.; Gheorghe, R.; Gruselle, M.; Ohkoshi, S. *J. Am. Chem. Soc.* **2009**, *131*, 16838−16843. (f) Gruselle, M.; Li, Y.; Ovanesyan, N.; Markhaev, V.; Shilov, G.; Mushenok, F.; Train, C.; Aldoshin, S. *Chirality* **2013**, *25*, 444−448.

(11) Clemente-León, M.; Coronado, E.; Gómez-García, C. J.; López-Jordà, M.; Camón, A.; Repollés, A.; Luis, F. *Chem.—Eur. J.* **2014**, *20*, 1669−1676.

(12) (a) Clemente-León, M.; Coronado, E.; Giménez-López, M. C.; Soriano-Portillo, A.; Waerenborgh, J. C.; Delgado, F. S.; Ruiz-Pérez, C. *Inorg. Chem.* **2008**, *47*, 9111−9120. (b) Clemente-León, M.; Coronado, E.; López-Jordà, M.; Mínguez Espallargas, G.; Soriano-Portillo, A.; Waerenborgh, J. C. *Chem.—Eur. J.* **2010**, *16*, 2207−2219. (c) Clemente-León, M.; Coronado, E.; López-Jordà, M. *Dalton Trans.* **2010**, *39*, 4903−4910. (d) Clemente-León, M.; Coronado, E.; López-Jordà, M.; Waerenborgh, J. C. *Inorg. Chem.* **2011**, *50*, 9122−9130. (e) Clemente-León, M.; Coronado, E.; López-Jordà, M.; Desplanches, C.; Asthana, S.; Wang, H.; Létard, J.-F. *Chem. Sci.* **2011**, *2*, 1121−1127. (f) Clemente-León, M.; Coronado, E.; López-Jordà, M. *Eur. J. Inorg. Chem.* **2013**, *2013*, 753−762. (g) Ben Djamâa, A.; Clemente-León, M.; Coronado, E.; López- Jordà, M. *Polyhedron* **2013**, *64*, 142−150. (h) Clemente-León, M.; Coronado, E.; López-Jordà, M.; Waerenborgh, J. C.; Desplanches, C.; Wang, H.; Létard, J.-F.; Hauser, A.; Tissot, A. *J. Am. Chem. Soc.* **2013**, *135*, 8655−8677.

(13) Coronado, E.; Galán-Mascarós, J. R.; Giménez-López, M. C.; Almeida, M.; Waerenborgh, J. C. *Polyhedron* **2007**, *26*, 1838−1844.

(14) (a) Atzori, M.; Benmansour, S.; Mínguez Espallargas, G.; Clemente-León, M.; Abhervé, A.; Gómez-Claramunt, P.; Coronado, E.; Artizzu, F.; Sessini, E.; Deplano, P.; Serpe, A.; Mercuri, M: L.; Gómez-García, C. J. *Inorg. Chem.* **2013**, *52*, 10031−10040. (b) Atzori, M.; Artizzu, F.; Sessini, E.; Marchiò, L.; Loche, D.; Serpe, A.; Deplano,

P.; Concas, G.; Pop, F.; Avarvari, N.; Mercuri, M: L. *Dalton Trans.* **2014**, *43*, 7006−7019.
(15) (a) Tweedle, M. F.; Wilson, L. J. *J. Am. Chem. Soc.* **1976**, *98*, 4824−4834. (b) Griffin, M.; Shakespeare, S.; Shepherd, H. J.; Harding, C. J.; Létard, J. F.; Desplanches, C.; Goeta, A. E.; Howard, J. A. K.; Powell, A. K.; Mereacre, V.; Garcia, Y.; Naik, A. D.; Müller-Bunz, H.; Morgan, G. G. *Angew. Chem., Int. Ed.* **2011**, *50*, 896−900.
(16) Nemec, I.; Herchel, R.; Salitros, I.; Trávnícek, Z.; Moncol, J.; Fuess, H.; Ruben, M.; Linert, W. *CrystEngComm* **2012**, *14*, 7015−7024.
(17) Sunatsuki, Y.; Ohta, H.; Kojima, M.; Ikuta, Y.; Goto, Y.; Matsumoto, N.; Iijima, S.; Akashi, H.; Kaizaki, S.; Dahan, F.; Tuchagues, J.-P. *Inorg. Chem.* **2004**, *43*, 4154−4171.
(18) Altomare, A.; Burla, M. C.; Camalli, M.; Cascarano, G. L.; Giacovazzo, C.; Guagliardi, A.; Moliterni, A. G. G.; Polidori, G.; Spagna, R. *J. Appl. Crystallogr.* **1999**, *32*, 115−119.
(19) Sheldrick, G. M. *Acta Crystallogr.* **2008**, *A64*, 112−122.
(20) Farrugia, L. J. *J. Appl. Crystallogr.* **2012**, *45*, 849−854.
(21) Spek, A. L. *J. Appl. Crystallogr.* **2003**, *36*, 7−13.
(22) (a) Kitagawa, S.; Kawata, S. *Coord. Chem. Rev.* **2002**, *224*, 11−34. (b) Michaelides, A.; Papadimitriou, C. D.; Plakatouras, J. C.; Skoulika, S.; Veltsistas, P. G. *Polyhedron* **2004**, *23*, 2587−2593. (c) Morikawa, S.; Yamada, T.; Kitagawa, H. *Chem. Lett.* **2009**, *38*, 654−655. (d) Yamada, T.; Morikawa, S.; Kitagawa, H. *Bull. Chem. Soc. Jpn.* **2010**, *83*, 42−48.
(23) Llunell, M.; Casanova, D.; Cirera, J.; Bofill, J. M.; Alemany, P.; Alvarez, S.; Pinski, M.; Avnir. D. *SHAPE*, version 2.0; University of Barcelona, 2010.
(24) Mínguez Espallargas, G.; Brammer, L.; Allan, D. R.; Pulha, C. R.; Robertson, N.; Warren, J. E. *J. Am. Chem. Soc.* **2008**, *130*, 9058−9071.
(25) Abhervé, A.; Clemente-León, M.; Coronado, E.; Gómez-García, C. J. Unpublished results.